Check for updates

# Accommodation capacity evaluation of renewable energy in power systems considering peak and frequency regulation

Yi Yu[1], Hongsheng Zhao[1], Yang Zeng[2]*, Feng Chen[1], Dongjun Yang[1], Bo Wang[1], Qiushi Xu[1] and Binxian Li[2]

[1]Economics and Technology Research Institute, State Grid Hubei Electric Power Co, Ltd., Wuhan, China, [2]College of Electrical and Information Engineering, Hunan University, Changsha, China

With the fast growth of renewable energy, the modern power systems are transitioning to the renewable energy dominated energy systems. However, the intrinsic intermittence and volatility of renewable energy also impose considerable challenges on the power system operation. Hence, it is of great significance to accurately evaluate the renewable energy accommodation capacity (REAC) in power system so as to effectively instruct the sustainable development of renewable energy and to alleviate the ongoing operational burdens. This paper proposes a novel evaluation method of REAC in power system comprehensively considering peak and frequency regulation. First, the mechanism and cost of deep peak regulation of thermal power units are deeply analyzed, and then the frequency dynamics response is modeled explicitly and simplified effectively. Next, a synthetic interaction model of "source-network-storage" is developed with diversified generation units, network and energy storage constraints. Furthermore, a multi-objective optimization model is established considering both economic and technical issues, and a REAC evaluation method is developed by integrating an incremental capacity augment approach with the proposed multi-objective model. Finally, the proposed REAC evaluation method is tested on the modified IEEE 39-bus system, and the numerical results verify the effectiveness of the proposed method.

KEYWORDS

renewable energy accommodation capacity, deep peak regulation, frequency dynamics response, "source-network-storage" interaction, multi-objective optimization model

# 1 Introduction

Driven by the promotion of the clean and sustainable development of energy system, there has been a proliferation of various renewable energy units, e.g. wind turbines (WT) and photovoltaic (PV) panels, in the power systems over the past years, leading to the transition of the power system structure and operating features to be increasingly complex (Khalkho et al., 2022; Majeed et al., 2022). Due to the significant inconsistency between

the generation pattern of renewable energy and the consumption pattern of load demand, the increasing integration of renewable energy exacerbates the difficulty for the peak shaving and valley filling of load, posing a substantial challenge to the peak regulation of the net load (You et al., 2022). Moreover, the replacement of conventional synchronous generation by the electronic-interfaced renewable energy generation will inevitably result in the continuous decline of power system inertia (Alves et al., 2021), which in turn weakens the frequency response ability to the emergencies and poses a serious threat to the power system stability. It has been reported that the present scale of renewable energy installation in some places of China has exceeded the accommodation capacity of its local power system, resulting in the substantial curtailment of wind power and photovoltaic power (Guo et al., 2020). Therefore, it is necessary to develop an effective evaluation method for accurate estimation of renewable energy accommodation capacity in order to provide a clear guidance for the progressive development and utilization of renewable energy.

Some efforts have been devoted to the investigation of renewable energy accommodation capacity (REAC) evaluation. To name it, the authors in (Lin et al., 2020) proposes a REAC evaluation method by simply considering the transmission line capacities in a power system simulation tool. In (He et al., 2018), peak load regulation and power equipment capacity limits have been identified as the key influencing factors of the REAC and based on this finding, an evaluation method is developed. In (Wang et al., 2016), an evaluation algorithm is proposed for the REAC based on sequential Monte Carlo simulation. Ref. (Zhang et al., 2019) uses the maximum flow model of network to study the REAC of power grid. Ref. (Chen et al., 2014) develops an assessment method for the renewable energy carrying capacity based on a stochastic long-term security constrained unit commitment model. However, the aforementioned research works oversimplify the various operating constraints of different devices, and also fail to account for the impact of deep peak regulation and frequency response on the evaluation outcome.

The interaction among power sources, network operator, load demand and energy storage exerts considerable influence on the REAC. Previously, most researchers merely focus on one simple aspect of the source-network-storage interaction. For instance, ref. (Xie et al., 2016) studies wind power accommodation capability from the perspective of network security. Ref. (Li et al., 2021) focuses on the correlation between wind power volatility and consumption capacity to evaluate the wind power consumption capacity. Ref. (Wang et al., 2018) investigates the power output model of WT and PV based on Copula theory to construct the REAC evaluation method. In (Xu et al., 2014), a probabilistic method is developed to determine the wind power accommodation capacity considering wind power and load scenarios. These works mainly focus on analyzing the influencing factors of renewable energy, and fail to account for the interaction among source, network, load and

storage as a whole. Therefore, to overcome this drawback, the interaction of "source-network-storage" is accurately modeled in detail and is seamlessly integrated in the REAC evaluation method.

In a word, most existing studies fail to account for the impact of peak regulation and frequency response requirements on the REAC, and also do not fully consider the interaction among "source-network-storage." To fill this research gap, this paper proposes an evaluation method of REAC considering peak regulation and frequency response requirements. First, the mechanism and cost of deep peak regulation of thermal power units is analyzed and then the frequency response dynamics is modeled explicitly and further simplified effectively. Subsequently, a comprehensive interaction model of "source-network-storage" is established with various generation, network and energy storage constraints. Finally, a novel REAC evaluation method is developed based on a proposed multi-objective optimization model considering both economic and technical issues. The contributions of this paper are three-fold as follows.

1) The peak regulation and frequency response requirements of power system are comprehensively incorporated in the proposed REAC evaluation method and explicitly modeled. Furthermore, to reduce computational complexity, the original complex peak regulation mechanism and frequency response dynamic are converted equivalently into several mathematically tractable mixed integer linear equations.

2) A multi-objective optimization model is established considering both the economic and technical issues in accommodating renewable energy, where the interaction among "source-network-storage" is fully considered to account for the realistic situation.

3) A novel REAC evaluation method is developed by integrating the above multi-objective optimization model with an incremental capacity augment approach. Consequently, the actual REAC which yields the lowest overall cost can be obtained efficiently and accurately.

The rest of this paper is arranged as follows. **Section 2** analyzes the peak regulation mechanism and frequency response requirement of the power system. **Section 3** constructs and analyzes a power system model considering "source-network-storage" interaction. **Section 4** presents a multi-objective optimization model of power system and a method to evaluate the accommodation capacity of renewable energy. In **Section 5**, the simulation is carried out and the numerical results are discussed. **Section 6** concludes the paper.

# 2 Peak and frequency regulation requirements

As is widely recognized, the high penetration of renewable energy in power system will aggravate the variation of net-load and thus increasing burden on peak load regulation.
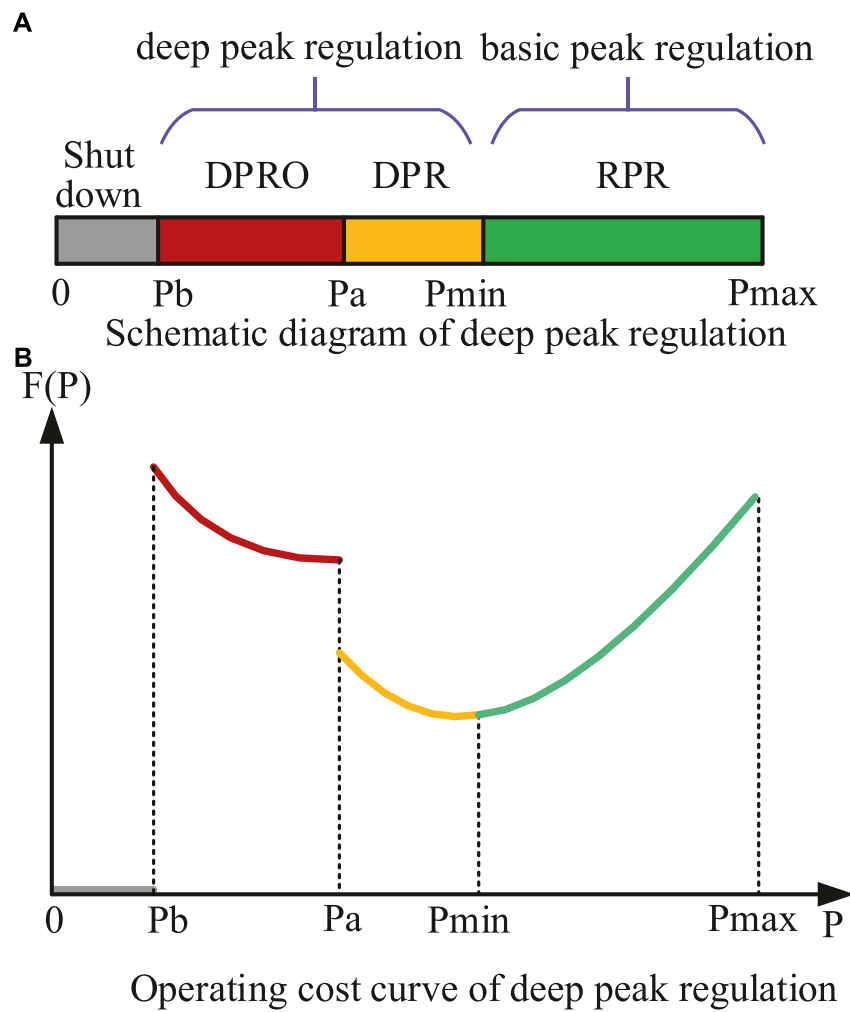
**FIGURE 1**
Deep peak regulation of thermal power unit. **(A)** Three states of peak regulation. **(B)** Overall operation cost curve in the deep peak regulation stage.

Furthermore, the replacement of conventional thermal generation by the electronic-interfaced renewable energy generation causes the significant decline of power system inertia, which places considerable stress on the frequency regulation. Therefore, it is necessary to deeply analyze the peak and frequency regulation requirements when evaluating the REAC.

## 2.1 Deep peak regulation mechanism

As conventional power generation units, e.g., thermal power units (TPU) and hydro units, are relatively more flexible in terms of regulation capacity compared with the renewable energy generation, they are the fundamental sources of peak regulation (Gao et al., 2020; Guan et al., 2022). The power output of the hydro units can be dropped to zero rapidly, while the thermal

power units are subject to the lower limits of the power output in order to maintain the on-state operation. When the thermal power units are invoked for the deep peak regulation, their minimum level of power outputs can be further lowered to achieve higher regulation capacity. However, the deep peak regulation by the thermal power units will cause additional cost and highly complex. In the following, we will thoroughly analyze the deep peak regulation mechanism and its cost composition.

### 2.1.1 Deep peak regulation mechanism of thermal power unit

The peak regulation process of TPU consists of three states, namely the regular peak regulation (RPR), the deep peak regulation without oil (DPR), and the deep peak regulation with oil (DPRO), as shown in **Figure 1A**, where $P_{max}$ is the upper limit of the unit power output; $P_{min}$ is the minimum technical power

output of the RPR state; $P_a$ is the minimum stable power output of the DPR state; $P_b$ is the minimum power output of the DPRO state. The operation costs of the thermal power unit during the deep peak regulation is composed of the coal consumption cost, tear-and-wear cost, oil input cost, and environmental pollution cost. The curve overall operation cost of thermal power unit considering deep peak regulation is shown in **Figure 1B**.

### 2.1.2 Deep peak regulation cost of thermal power unit

As can be seen from **Figure 1**, the operation cost of thermal power units is highly related to the deep peak regulation states. If the TPU is in the RPR state, its operation cost only consists of coal consumption cost. When the TPU is in the DPR and DPRO states, its power output deviates from the normal range leading to the accelerated aging of mechanical parts and shortening of its life cycle. Thus, in addition to the coal consumption cost, the TPU operation cost in the DPR and DPRO states also includes the tear-and-wear cost. When a TPU is operated in DRRO state, additional oil input is required to maintain the steady operation of the units, which will further cause environmental pollution. Hence, the costs of oil fuel and environment pollution should be taken into account. Therefore, the TPU operation cost in deep peak regulation state consists of coal consumption cost $C_{i,t}^{coal}$, tear-and-wear cost $C_{i,t}^{abr}$, fuel cost $C_{i,t}^{oil}$ and additional environment pollution cost $C_{i,t}^{ev}$, as illustrated by the following equations.

$$C_{i,t}^{coal} = a_i\left(P_{i,t}^g\right)^2 + b_i P_{i,t}^g + c_i \qquad \forall i \in N_g, \forall t \in T \qquad (1a)$$

$$C_{i,t}^{abr} \approx \frac{\beta S_i^g}{\left[2N_f\left(P_{i,t}^g\right)\right]} \qquad \forall i \in N_g, \forall t \in T \qquad (1b)$$

$$N_f\left(P_{i,t}^g\right) = 0.005778\left(P_{i,t}^g\right)^3 - 2.682\left(P_{i,t}^g\right)^2 + 484.8 P_{i,t}^g - 8411 \qquad \forall i \in N_g, \forall t \in T \qquad (1c)$$

$$C_{i,t}^{oil} = \gamma_{oil} Q_i^{oil} \qquad \forall i \in N_g, \forall t \in T \qquad (1d)$$

$$C_{i,t}^{ev} = \Delta\mu_{env,i}\omega_{env} \qquad \forall i \in N_g, \forall t \in T \qquad (1e)$$

**Eq. 1a** is the quadratic coal consumption cost of TPU $i$ at the time $t$, where $P_{i,t}^g$ is the power output; $a_i$, $b_i$, and $c_i$ are the cost coefficients. **Eq. 1b** approximates the tear-and-wear cost of TPU based on the commonly used Manson-Coffin formula, where $\beta$ is a cost conversion coefficient; $S_i^g$ is the overall investment cost of TPU $i$, and $N_f(P_{i,t}^g)$ is the number of rotor cracking cycles. **Eq. 1c** is the calculation formula of rotor cracking cycles number, which is a cubic equation of power output. **Eq. 1d** shows that the oil consumption cost, where $Q_i^{oil}$ is the amount of oil fuel consumption and $\gamma_{oil}$ is the price of oil fuel. **Eq. 1e** shows additional environment pollution surcharge during

DRPO, where $\Delta\mu_{env,i}$ and $\omega_{env}$ are the amount of additional emission caused by DPRO and the unit penalty for environment pollution, respectively.

Based on the discussed above, the overall operation cost of TPU in deep peak regulation can be expressed as **Eq. 2**.

$$F_{i,t}^g = \begin{cases} C_{i,t}^{coal} & \text{if } \underline{P_i^g} < P_{i,t}^g < \overline{P_i^g} \\ C_{i,t}^{coal} + C_{i,t}^{abr} & \text{if } P_i^{ga} < P_{i,t}^g < \underline{P_i^g} \\ C_{i,t}^{coal} + C_{i,t}^{abr} + C_{i,t}^{oil} + C_{i,t}^{env} & \text{if } P_i^{gb} < P_{i,t}^g < P_i^{ga} \end{cases} \quad \forall i \in N_g, \forall t \in T$$
$$(2)$$

where $F_{i,t}^g$ is the overall operation cost of TPU $i$ at the time $t$; $\overline{P_i^g}$ and $\underline{P_i^g}$ are the upper and lower power limit of TPU $i$ in the RPR state; $P_i^{ga}$ is the lower power limit of TPU $i$ in the DPR state; $P_i^{gb}$ is the lower power limit of TPU $i$ in the DPRO stage.

### 2.1.3 The linearization of deep peak regulation cost

It can be seen from (1) and (2) the coal consumption cost $C_{i,t}^{coal}$, tear-and-wear cost $C_{i,t}^{abr}$, and the overall operation cost $F_{i,t}^g$ are nonlinear, which results in the significant computational complexity. Hence, those terms need to be linearized for computational simplicity.

Both $C_{i,t}^{coal}$ and $C_{i,t}^{abr}$ are nonlinear functions of the single variable (the active power output $P_{i,t}^g$), which can be linearized using piecewise linearization (PWL) technology (Carrión and Arroyo, 2006). For brevity, $C_{i,t}^{coal}$ and $C_{i,t}^{abr}$ are first generalized as a nonlinear function of a single variable $F(a)$ and then $F(a)$ is further linearized as follows,

$$F(a) \approx F(a_1) + \sum_{k=1}^{K}\left[F(a_{k+1}) - F(a_k)\right]\delta_k \qquad (3a)$$

$$a = a_1 + \sum_{k=1}^{K}\left(a_{k+1} - a_k\right)\delta_k \qquad (3b)$$

$$\delta_{k+1} \le \sigma_k \le \delta_k \qquad k \in \{1, \ldots, K-1\} \qquad (3c)$$

$$0 \le \delta_k \le 1 \qquad k \in \{1, \ldots, K\} \qquad (3d)$$

where $a$ is the input single variable of the function $F(a)$ and its range is divided into $K$ segments; $a_k$ and $a_{k+1}$ are the two endpoints of the $k$th segment; $\delta_k$ is a continuous variable that represents the portion of the $k$th segment; $\sigma_{k-1}$ is an auxiliary binary variable that indicates whether $a$ lies on the right-side of the $k$th segment.

The overall operation cost $F_{i,t}^g$ is not only related to the active power output $P_{i,t}^g$, but also related to the deep peak regulation state. Hence, the cost $F_{i,t}^g$ can be reformulated as **Eqs 4a, 4b** by introducing several binary variables $U_{i,t}^{g1}$, $U_{i,t}^{g2}$, $U_{i,t}^{g3}$ and $X_{i,t}^g$.

$$F_{i,t}^g = X_{i,t}^g C_{i,t}^{coal} + \left(U_{i,t}^{g2} + U_{i,t}^{g3}\right)C_{i,t}^{abr} + U_{i,t}^{g3}C_{i,t}^{oil} + U_{i,t}^{g3}C_{i,t}^{env} \qquad \forall i \in N_g, \forall t \in T \qquad (4a)$$
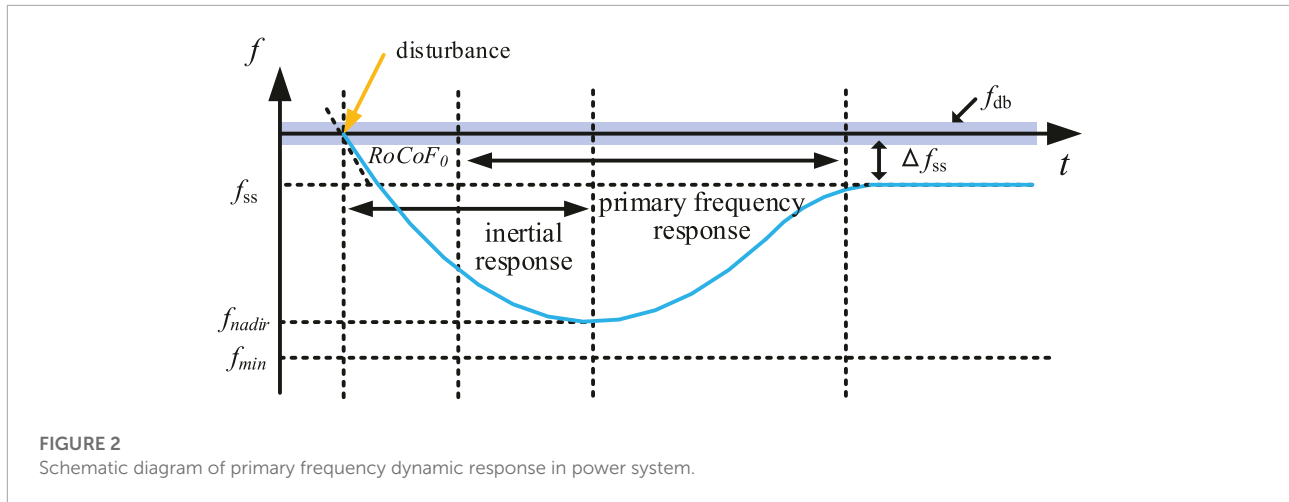
**FIGURE 2**
Schematic diagram of primary frequency dynamic response in power system.

$$U_{i,t}^{g1} + U_{i,t}^{g2} + U_{i,t}^{g3} = X_{i,t}^{g} \qquad \forall i \in N_g, \forall t \in T \qquad (4b)$$

where $U_{i,t}^{g1}$, $U_{i,t}^{g2}$ and $U_{i,t}^{g3}$ indicate the different peak regulation states; $X_{i,t}^{g}$ denotes the on or off state. If the TPU $i$ has been turned on at time $t$, $X_{i,t}^{g}$ is equal to 1; otherwise it is equal to 0. If the unit $i$ is in the RPR state, $U_{i,t}^{g1} = 1$, otherwise it is equal to 0; if the unit $i$ is in the DPR state, $U_{i,t}^{g2} = 1$, otherwise it is equal to 0; if the unit $i$ is in the DPRO state, $U_{i,t}^{g3} = 1$, otherwise it is equal to 0. If the TPU $i$ has been turned off at time $t$, $U_{i,t}^{g1}$, $U_{i,t}^{g2}$ and $U_{i,t}^{g3}$ are enforced to be 0 due to **Eq. 4b**.

The first two terms of **Eq. 4a** are nonlinear, which can be linearized using big M method. **Eq. 4a** can be reformulated as mixed integer linear equation as follows,

$$F_{i,t}^{g} = C_{i,t}^{Xcoal} + C_{i,t}^{Xabr} + U_{i,t}^{g3} C_{i,t}^{oil} + U_{i,t}^{g3} C_{i,t}^{env} \qquad \forall i \in N_g, \forall t \in T \qquad (5a)$$

$$\begin{cases} X_{i,t}^{g} C_{i,min}^{coal} \le C_{i,t}^{Xcoal} \le X_{i,t}^{g} C_{i,max}^{coal} \\ C_{i,t}^{coal} - \left(1 - X_{i,t}^{g}\right) M \le C_{i,t}^{Xcoal} \le C_{i,t}^{coal} + \left(1 - X_{i,t}^{g}\right) M \end{cases} \qquad \forall i \in N_g, \forall t \in T \qquad (5b)$$

$$\begin{cases} \left(U_{i,t}^{g2} + U_{i,t}^{g3}\right) C_{i,min}^{abr} \le C_{i,t}^{Xabr} \le \left(U_{i,t}^{g2} + U_{i,t}^{g3}\right) C_{i,max}^{abr} \\ C_{i,t}^{abr} - \left(1 - \left(U_{i,t}^{g2} + U_{i,t}^{g3}\right)\right) M \le C_{i,t}^{Xabr} \le C_{i,t}^{abr} + \left(1 - \left(U_{i,t}^{g2} + U_{i,t}^{g3}\right)\right) M \end{cases} \qquad \forall i \in N_g, \forall t \in T \qquad (5c)$$

where $C_{i,t}^{Xcoal}$, $C_{i,t}^{Xabr}$ are new variables representing $X_{i,t}^{g} C_{i,t}^{coal}$ and $(U_{i,t}^{g1} + U_{i,t}^{g2}) C_{i,t}^{abr}$, respectively; $M$ is a large number.

## 2.2 Frequency response requirements

The frequency response dynamic reflects the instantaneous power balance. When a large power disturbance occurs, the frequency may fall too fast or deviate too far from the nominal value if the frequency response requirement is not appropriated considered, which will further trigger the action of under frequency load shedding (UFLS) relay resulting in serious power

accidents. In order to make the system have sufficient inertia support and maintain the frequency dynamic stability, the frequency dynamic response should be taken into account during REAC evaluation (Kushwaha et al., 2018).

### 2.2.1 Primary frequency response constraints

The frequency response process includes inertial response, primary frequency response (PFR), secondary and tertiary responses (Teng and Strbac, 2016). Since three key performance indices of frequency response, including rate of change of frequency $RoCoF$, frequency level at nadir $f_{nadir}$, and frequency deviation level at quasi-steady state $\Delta f_{ss}$, are only related to the inertial response and PFR as shown in **Figure 2**, secondary and tertiary responses are not considered in this paper. Specifically, $RoCoF$ reflects the rate of change in the frequency, $f_{nadir}$ reflects the largest frequency deviation during frequency response dynamic, and $\Delta f_{ss}$ reflects the regulation effect of PFR at the stead state.

The frequency response dynamic is affected by multiple factors, including system inertia, load variation, generator governor response, which results in a highly complex process. In order to reduce the computational complexity, the load damping rate is ignored. The frequency dynamics of the simplified system can be expressed by **Eq. 6**.

$$2 \frac{H_t^{sys}}{f_0} \frac{d\Delta f}{dt} = \frac{\Delta P_m - \Delta P_e}{S_b} \qquad (6)$$

where $\Delta f$ is the frequency deviation; $f_0$ is the rated frequency, $S_b$ is the system capacity base; $H_t^{sys}$ is the system inertia constant at the time $t$; $\Delta P_m$ and $\Delta P_e$ are the mechanical power output and electrical power output of the system, respectively. In this paper, thermal power unit, hydro-power unit and pumped storage unit with inherent inertia are considered to participate in the primary frequency response.

### 2.2.1.1 RoCoF limits

When an disturbance occurs, the power imbalance - $\Delta P_L$ will arise which is equal to the difference between the change of system mechanical power output and electrical power output $\Delta P_m$ - $\Delta P_e$. The RoCoF reaches the maximum at the occurrence of the interference according to (6), which is related to the system inertia and power imbalance (Wen et al., 2016). In order to prevent the triggering of UFLS relay caused by the too fast change of frequency, $RoCoF$ should be maintained below a certain level $RoCoF_{max}$, as illustrated by the following equations.

$$RoCoF_0 = \frac{d\Delta f}{dt} = -\frac{\Delta P_L f_0}{2H_t^{sys} S_b} \tag{7a}$$

$$|RoCoF| \le RoCoF_{max} \tag{7b}$$

Since $H_t^{sys}$ is the total inertia of all remaining online units in the system, the operation status of the units needs to be optimized to ensure that the system has sufficient units to provide inertia support after disturbance. Therefore, constraints (7) can be converted into the following linear constraint with respect to the unit status.

$$H_t^{sys} = \frac{\sum_{i=1}^{N_k} H_i^{gen} P_i^{genmax} X_i^{genN}}{S_b} \ge \frac{\Delta P_L f_0}{2 S_b RoCoF_{max}} \tag{8}$$

where $H_i^{gen}$ and $P_i^{genmax}$ denote the inertia constant and the maximum power output of the generator unit $i$, respectively; $X_i^{genN}$ is the operation status of the generator unit $i$; $N_k$ is the set of generator units that have rotational inertia.

### 2.2.1.2 Frequency nadir limits

The frequency level at nadir $f_{nadir}$ is related to factors such as system inertia, governor response, and governor dead zone. In order to ensure the frequency does not fall below the minimum frequency requirement $f_{min}$ or exceed the maximum frequency requirement $f_{max}$ specified by the UFLS relay, the generator units involved in PFR should reserve sufficient frequency regulation capacity (Chávez et al., 2014). Meanwhile, the reserves of each unit participating in PFR should be delivered at or before the frequency level at nadir $f_{nadir}$. Therefore, the reserve of each unit should not exceed an upper limit, so that the governor of each unit can respond rapidly and counteract the frequency deviation before the frequency exceeds the limit of the UFLS relay (Zhang et al., 2018). The constraints of the downward and upward reserves ($RU_{i,t}$ and $RU_{i,t}$) of each unit after reformulation are demonstrated as follows,

$$RU_{i,t} \le 2c_i^R \frac{2H_t^{sys} S_b (f_0 - f_{min} - f_{db})}{f_0 \Delta P_L} \tag{9a}$$

$$RD_{i,t} \le 2c_i^R \frac{2H_t^{sys} S_b (-f_0 + f_{max} - f_{db})}{f_0 \Delta P_L} \tag{9b}$$

where $f_{db}$ is the frequency response dead-band of the governor, and $c_i^R$ is the maximum ramping rate of the unit $i$'s governor.

### 2.2.1.3 Frequency level limits at quasi steady state

After the generation units deliver the reserves, the system frequency will gradually recover, and then enter the quasi-steady state, so that the primary frequency response stage ends. The quasi-stable state frequency $\Delta f_{ss}$ of the power system is related to the system droop coefficient $K_s$ and interference power $\Delta P_L$.

$$|\Delta f_{ss} = -\frac{\Delta P_L}{K_s}| \le \Delta f_{ss}^{max} \tag{10a}$$

$$K_s = K_G + K_D = \frac{\sum_{i=1}^{N_k} K_{G,i}^\star P_i^{genN} X_{i,t}^{genN}}{f_0} + \frac{K_D^\star P_t^D}{f_0} \tag{10b}$$

where $\Delta f_{ss}^{max}$ is the maximum allowable frequency deviation of quasi-steady state; $K_G$ and $K_G^\star$ are the actual value and per-unit value of the droop coefficient of unit $i$, respectively; $K_D$ and $K_D^\star$ are the actual value and per-unit value of the load damping constant, respectively; $P_i^{genN}$ and $X_{i,t}^{genN}$ are the rated active power and on/off state of unit $i$, respectively; $P_t^D$ is the total load at time $t$.

## 3 Interaction modeling of "source-network-storage"

As previously discussed, in order to improve the REAC, it is necessary to take into account the interaction among various power sources, network and energy storage. To this end, detailed models of multiple types of power generation including TPU, hydro-power plant (HPP), wind farm and PV farm, energy storage systems including battery energy storage station (BES) and pumped storage power station (PSP) as well as transmission network are established in the following. **Figure 3** demonstrates a graphical representation of modern power system with various power sources and energy storage systems, where the interaction of "source-network-storage" is achieved through power system scheduling.

## 3.1 Modeling of various power sources

### 3.1.1 Thermal power unit

With the increasing penetration of renewable energy, the role of TPU is changing from conventional energy supplier to the flexibility provider in order to accommodate renewable energy in power systems. The operational constraints of TPU are formulated as follows,

$$U_{i,t}^{g1}\underline{P_i^g} + U_{i,t}^{g2}P_i^{ga} + U_{i,t}^{g3}P_i^{gb} \le P_{i,t}^g \le X_{i,t}^g \overline{P_i^g} \qquad \forall i \in N_g, \forall t \in T \tag{11a}$$

$$X_{i,t}^g - X_{i,t-1}^g \le X_{i,\tau}^g \qquad \forall i \in N_g, \tau \in [t+1, min\{t+MinUp_i-1, T\}], t \in [2, T] \tag{11b}$$
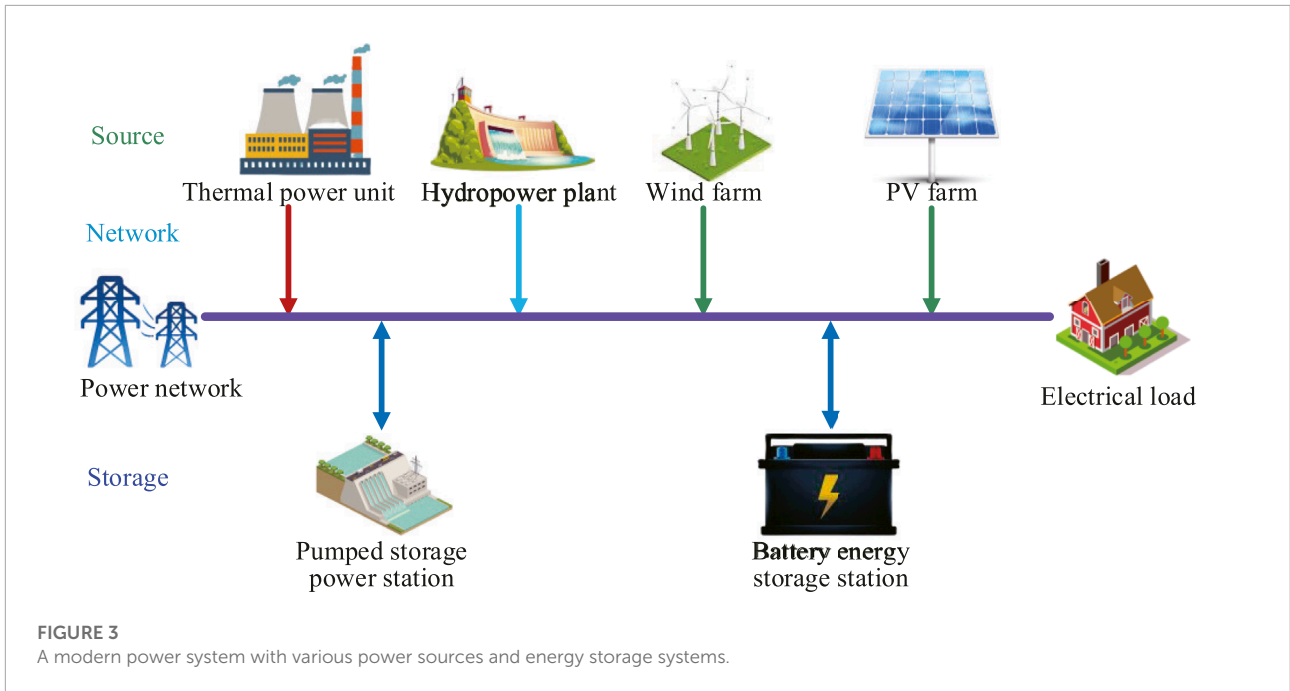
**FIGURE 3**
A modern power system with various power sources and energy storage systems.

$$X_{i,t-1}^g - X_{i,t}^g \leq 1 - X_{i,\tau}^g \quad \forall i \in N_g, \tau \in [t+1, min\{t + MinDw_i - 1, T\}], t \in [2, T] \tag{11c}$$

$$P_{i,t}^g - P_{i,t-1}^g <= Y_{i,t}^g P_i^{gsu} + X_{i,t-1}^g R_i^{up} \qquad \forall i \in N_g, \forall t \in T \tag{11d}$$

$$P_{i,t-1}^g - P_{i,t}^g <= Z_{i,t}^g P_i^{gsd} + X_{i,t}^g R_i^{dw} \qquad \forall i \in N_g, \forall t \in T \tag{11e}$$

$$X_{i,t}^g - X_{i,t-1}^g = Y_{i,t}^g - Z_{i,t}^g \qquad \forall i \in N_g, \forall t \in T \tag{11f}$$

$$Y_{i,t}^g + Z_{i,t}^g \leq 1 \qquad \forall i \in N_g, \forall t \in T \tag{11g}$$

$$RU_{i,t}^g \leq min\left\{X_{i,t}^g \overline{P}_i^g - P_{i,t}^g, R_i^{up}\right\} \qquad \forall i \in N_g, \forall t \in T \tag{11h}$$

$$RD_{i,t}^g \leq min\left\{P_{i,t}^g - \left(U_{i,t}^{g1}\underline{P}_i^g + U_{i,t}^{g2}P_i^{ga} + U_{i,t}^{g3}P_i^{gb}\right), R_i^{dw}\right\} \qquad \forall i \in N_g, \forall t \in T \tag{11i}$$

Constraint (11a) imposes the power output limits on TPU considering the deep peak regulation. Constraints (11b) and (11c) enforce the minimum on time limits and minimum off time limits, where $MinUp_i$ and $MinDw_i$ are the minimum on time limit and minimum off time limit, respectively; $T$ denotes the operation horizon, which is divided into $T$ time intervals with the duration of each time interval being 1 h. Constraints (11d) and (11e) describe the ramp rate limit of TPU, where $R_i^{up}$, $R_i^{dw}$ are the ramp-up and ramp-down rate limits, respectively; $P_i^{gsu}$, $P_i^{gsd}$ are the minimum startup and shutdown power limit, respectively; $Y_{i,t}^g$ and $Z_{i,t}^g$ are the startup and shutdown indicator variables at time $t$, respectively. The

logical relationship between startup/shutdown indicators and on/off state variables is represented by constraints (11f) and (11g). When the TPU $i$ starts up at time $t$, $Y_{i,t}^g = 1$, otherwise it is 0; when the TPU $i$ shuts down at time $t$, $Z_{i,t}^g = 1$, otherwise it is 0. Constraints (11h) and (11i) show the limits of the upward and downward reserves, where $RU_{i,t}^g$ and $RD_{i,t}^g$ are the upward and downward reserves at time $t$, respectively.

### 3.1.2 Hydro-power plant

As one of major power sources, HPP can be flexibly dispatched to meet the peak and frequency regulation requirements. The HPP mainly includes the following operational constraints.

$$\underline{V}_h \leq V_{h,t} \leq \overline{V}_h \qquad \forall h \in N_h, \forall t \in T \tag{12a}$$

$$V_{h,0} = v_{h,0}, V_{h,T} = v_{h,T} \qquad \forall h \in N_h, \forall t \in T \tag{12b}$$

$$V_{h,t} = V_{h,t-1} + Qn_{h,t} - Q_{h,t} - SQ_{h,t} \qquad \forall h \in N_h, \forall t \in T \tag{12c}$$

$$u_{h,t}^{hy}\underline{Qb}_h \leq Q_{h,t} + SQ_{h,t} \leq u_{h,t}^{hy}\overline{Qb}_h \qquad \forall h \in N_h, \forall t \in T \tag{12d}$$

$$u_{h,t}^{hy}\underline{P}_h \leq P_{h,t} \leq u_{h,t}^{hy}\overline{P}_h \qquad \forall h \in N_h, \forall t \in T \tag{12e}$$

$$P_{h,t}^h = g\eta_h Q_{h,t} H_{h,t} \qquad\qquad \forall h \in N_h, \forall t \in T \tag{12f}$$

$$H_{h,t} = Hd_{h,0} + \alpha_h V_{h,t} \qquad\qquad \forall h \in N_h, \forall t \in T \tag{12g}$$

$$RU_{h,t}^{hy} \le u_{h,t}^{hy} \overline{P}_h - P_{h,t} \qquad\qquad \forall h \in N_h, \forall t \in T \tag{12h}$$

$$RD_{h,t}^{hy} \le P_{h,t} - u_{h,t}^{hy} \underline{P}_h \qquad\qquad \forall h \in N_h, \forall t \in T \tag{12i}$$

$$u_{h,t}^{hy} - u_{h,t-1}^{hy} = Y_{h,t}^{hy} - Z_{h,t}^{hy} \qquad\qquad \forall h \in N_h, \forall t \in T \tag{12j}$$

$$Y_{h,t}^{hy} + Z_{h,t}^{hy} \le 1 \qquad\qquad \forall h \in N_h, \forall t \in T \tag{12k}$$

Constraints (12a) and (12b) impose the limits of reservoir capacity, where $V_{h,t}$ is the reservoir storage capacity at time $t$; $\overline{V}_h$ and $\underline{V}_h$ are the upper and lower limits of reservoir capacity, respectively; $v_{h,0}$ and $v_{h,T}$ represent the initial and final reservoir capacity of the entire operation horizon, respectively. Constraint (12c) describes the conservation law of water mass, where $Qn_{h,t}$ and $SQ_{h,t}$ are the natural flow into the reservoir and the spillage of HPP $h$, respectively; $Q_{h,t}$ is the water flow for generation. Constraint (12d) enforces the limits on the water discharge, where $\overline{Qb}_h$ and $\underline{Qb}_h$ are the upper and lower limits of discharge water flow, respectively; $u_{h,t}$ is the on/off state variable of HPP. Constraint (12e) shows the power output limits of HPP, where $P_{h,t}$ is power output; $\overline{P}_h$ and $\underline{P}_h$ are the upper and lower limits of power output, respectively; Constraint (12f) is the hydraulic conversion function of HPP, which describes the relationship between power generation, water head and water flow, where $H_{h,t}$ is the water head of HPP $h$ at time $t$; $g$ is the gravity coefficient, $\eta_h$ is the energy conversion efficiency. Constraint (12g) shows the short-term relationship between water head and reservoir capacity, where $Hd_{h,0}$ and $\alpha_h$ are the correlation coefficients between water head and reservoir capacity. Constraints (12h) and (12i) illustrates the upward and downward reserves capacity of HPP, where $RU_{h,t}^{hy}$ and $RD_{h,t}^{hy}$ are the upward and downward reserves at time $t$, respectively. The logical relationship between startup/shutdown indicator variables and on/off state variable of HPP is represented by constraints (12j) and (12k), where $Y_{h,t}^{hy}$ and $Z_{h,t}^{hy}$ are the startup and shutdown indicators of the HPP $h$ at time $t$, respectively.

Since constraint (Eq. 12f) is nonlinear, in order to reduce computational complexity, the linearization method in (Babayev, 1997; Wu et al., 2008) is adopted. For HPP, constraint (Eq. 12g) is incorporated into constraint (Eq. 12f) to obtain the

hydraulic conversion formula as $P_{h,t}^h = g\eta_h Q_{h,t}(Hd_{h,0} + \alpha_h V_{h,t})$. By dividing $Q_{h,t}$ and $V_{h,t}$ into subintervals $[Q_i, Q_{i+1}]$ and $[V_j, V_{j+1}]$, the hydraulic conversion equation is split into a grid of $(m-1)$ () $(n-1)$ in which each point corresponding to the original function is $P_{i,j} = g\eta_h Q_i (Hd_{h,0} + \alpha_h V_j)$, where $i = 1,\ldots,m-1$, $j = 1,\ldots,n-1$. Consequently, the constraint (Eq. 12f) is transformed into linear Equation 13 by introducing several auxiliary variables.

$$Q_{h,t} = \sum_{i=1}^m \sum_{j=1}^n Q_i \cdot \phi_{i,j}, V_{h,t} = \sum_{i=1}^m \sum_{j=1}^n V_j \cdot \phi_{i,j} \tag{13a}$$

$$\sum_{i=1}^m \sum_{j=1}^n \left(\zeta_{i,j} + \xi_{i,j}\right) = 1 \qquad \zeta_{i,j}, \xi_{i,j} \in \{0,1\} \tag{13b}$$

$$\sum_{i=1}^m \sum_{j=1}^n \phi_{i,j} = 1 \qquad\qquad \phi_{i,j} \ge 0 \tag{13c}$$

$$\phi_{i,j} \le \zeta_{i,j-1} + \zeta_{i,j} + \zeta_{i,j+1} + \xi_{i-1,j} + \xi_{i,j} + \xi_{i+1,j} \tag{13d}$$

$$P_{h,t}^h = \sum_{i=1}^m \sum_{j=1}^n P_{i,j} \cdot \phi_{i,j} \tag{13e}$$

### 3.1.3 Renewable energy generation

The renewable energy is less flexible in power output adjustment. When it is required by the system operator, the renewable energy like PV and WT can be curtailed to maintain the power balance. The operational constraints of WT and PV mainly include:

$$0 \le \Delta P_{m,t}^{wt} \le P_m^{wt} \qquad\qquad \forall m \in N_{wt}, \forall t \in T \tag{14a}$$

$$0 \le \Delta P_{n,t}^{pv} \le P_n^{pv} \qquad\qquad \forall n \in N_{pv}, \forall t \in T \tag{14b}$$

constraints (14a) and (14b) illustrate the curtailment of wind power and PV power should not exceed their predicted output, where $\Delta P_{m,t}^{wt}$ and $\Delta P_{n,t}^{pv}$ are the curtailments of wind power and PV power, respectively; $P_{m,t}^{wt}$, $P_{n,t}^{pv}$ are the predicted WT output and PV output at time $t$, respectively.

## 3.2 Modeling of energy storage systems

The rapid development energy storage technology especially the battery energy storage provides a promising solution for the renewable energy accommodation problem. In this subsection, the operational models of both battery energy storage systems and pumped storage power station are established.

### 3.2.1 Battery energy storage

The flexible and rapid adjustment capability of BES can be deployed to provide peak regulation and frequency regulation support (Tan and Zhang, 2017; Carrión et al., 2018). The operational model of BES mainly includes the following constraints.

$$0 \le P_{s,t}^{ch} \le W_{s,t}^{BES} \overline{P}_s^{ch} \qquad \forall s \in N_{BES}, \forall t \in T \qquad (15a)$$

$$0 \le P_{s,t}^{dis} \le \left(1 - W_{s,t}^{BES}\right) \overline{P}_s^{dis} \qquad \forall s \in N_{BES}, \forall t \in T \qquad (15b)$$

$$SOC_{s,t} = SOC_{s,t-1} + \left( \eta^{ch} P_{s,t}^{ch} - \frac{P_{s,t}^{dis}}{\eta^{dis}} \right) / C_s^{BES} \Delta T \qquad \forall s \in N_{BES}, \forall t \in T \qquad (15c)$$

$$\underline{SOC}_s \le SOC_{s,t} \le \overline{SOC}_s \qquad \forall s \in N_{BES}, \forall t \in T \qquad (15d)$$

Constraints (15d) and (15b) describe the charge and discharge power limits of BES, where $P_{s,t}^{ch}$ and $P_{s,t}^{dis}$ are charging, discharging power at time $t$, respectively; $\overline{P}_s^{ch}$ and $\overline{P}_s^{dis}$ are the upper limits of charging and discharging power, respectively; $W_{s,t}^{BES}$ is the logical variable that indicates the charging and discharging state of BES $s$ at the time $t$; $W_{s,t}^{BES} = 1$ indicates that it is in the charge state; $W_{s,t}^{BES} = 0$ indicates that it is in the discharge state. Note that the simultaneous charging and discharging is forbidden by Eqs 15a, 15b. Constraint (15c) describes the variation of state of charge (SOC), where $SOC_{s,t}$ is the SOC of BES $s$ at time $t$; $C_s^{BES}$ is the energy storage capacity of BES $s$; $\eta^{ch}$ and $\eta^{dis}$ are the charging and discharging efficiency of BES $s$, respectively. Constraint (15d) indicates that SOC of BES needs to be maintained within the allowable range, where $\underline{SOC}_s$ and $\overline{SOC}_s$ are the upper and lower limit of SOC, respectively; $\Delta T$ denotes the time interval of the operation horizon $T$ with a duration of 1 h.

### 3.2.2 Pumped storage power station

The PSP can be operated in either generating mode or pumping mode (Xia et al., 2019; Liu et al., 2021). Different operation modes can be switched smoothly. Thus, it is effective device for the peak shaving and valley filling of power system. The operational model of PSP consists of the following constraints. For brevity, we will define the subscriptions, superscriptions and several commonly used notations first and no longer illustrate those afterwards. Specifically, subscriptions $p$ and $g$ denote the indices of the pumped storage power station and pumped generation units with a PSP, respectively; Superscriptions $pg$ and $ph$ denote the generating mode and pumping mode, respectively; $u$ denotes the operation state of the PSP or the unit; $Y$ and $Z$ represent the startup and shutdown indicators of the PSP unit, respectively.

$$u_{p,t}^{pg} + u_{p,t}^{ph} \le 1 \qquad \forall p \in N_{PS}, \forall t \in T \qquad (16a)$$

$$u_{p,g,t}^{pg} \le u_{p,t}^{pg}, u_{p,g,t}^{ph} \le u_{p,t}^{ph} \qquad \forall p \in N_{PS}, \forall g \in N_p^{gu}, \forall t \in T \qquad (16b)$$

$$u_{p,g,t}^{pg} \underline{P}_{p,g}^{pg} \le P_{p,g,t}^{pg} \le u_{p,g,t}^{pg} \overline{P}_{p,g}^{pg} \qquad \forall p \in N_{PS}, \forall g \in N_p^{gu}, \forall t \in T \qquad (16c)$$

$$u_{p,g,t}^{ph} \underline{P}_{p,g}^{ph} \le P_{p,g,t}^{ph} \le u_{p,g,t}^{ph} \overline{P}_{p,g}^{ph} \qquad \forall p \in N_{PS}, \forall g \in N_p^{gu}, \forall t \in T \qquad (16d)$$

$$RC_{p,t} = RC_{p,t-1} + \left( \sum_{g=1}^{N_p^{gu}} \eta_{ph} P_{p,g,t}^{ph} - \sum_{g=1}^{N_p^{gu}} \eta_{pg} P_{p,g,t}^{pg} \right) \Delta T \qquad \forall p \in N_{PS}, \forall t \in T \qquad (16e)$$

$$\underline{RC}_p \le RC_{p,t} \le \overline{RC}_p \qquad \forall p \in N_{PS}, \forall t \in T \qquad (16f)$$

$$RC_{p,T} = RC_{p,0} \qquad \forall p \in N_{PS} \qquad (16g)$$

$$u_{p,g,t}^{pg} - u_{p,g,t-1}^{pg} = Y_{p,g,t}^{pg} - Z_{p,g,t}^{pg} \qquad \forall p \in N_{PS}, \forall g \in N_p^{gu}, \forall t \in T \qquad (16h)$$

$$Y_{p,g,t}^{pg} + Z_{p,g,t}^{pg} \le 1 \qquad \forall p \in N_{PS}, \forall g \in N_p^{gu}, \forall t \in T \qquad (16i)$$

$$u_{p,g,t}^{ph} - u_{p,g,t-1}^{ph} = Y_{p,g,t}^{ph} - Z_{p,g,t}^{ph} \qquad \forall p \in N_{PS}, \forall g \in N_p^{gu}, \forall t \in T \qquad (16j)$$

$$Y_{p,g,t}^{ph} + Z_{p,g,t}^{ph} \le 1 \qquad \forall p \in N_{PS}, \forall g \in N_p^{gu}, \forall t \in T \qquad (16k)$$

$$RU_{p,g,t}^{PS} \le u_{p,g,t}^{pg} \overline{P}_{p,g}^{pg} - P_{p,g,t}^{pg} + P_{p,g,t}^{ph} - u_{p,g,t}^{ph} \underline{P}_{p,g}^{ph} \qquad \forall p \in N_{PS}, \forall g \in N_p^{gu}, \forall t \in T \qquad (16l)$$

$$RD_{p,g,t}^{PS} \le u_{p,g,t}^{ph} \overline{P}_{p,g}^{ph} - P_{p,g,t}^{ph} + P_{p,g,t}^{pg} - u_{p,g,t}^{pg} \underline{P}_{p,g}^{pg} \qquad \forall p \in N_{PS}, \forall g \in N_p^{gu}, \forall t \in T \qquad (16m)$$

Constraint (16a) ensures the simultaneous pumping and generating states of PSP is avoided. Constraint (16b) illustrates the operation states of internal units of PSP are consistent with operation state of the station. Constraints (16c) and (16d) impose the power generation limits and pumping power limits on individual PSP units, respectively, where $\underline{P}^{pg}/\overline{P}^{pg}$ is the minimum/maximum generating power of the unit; $\underline{P}^{ph}/\overline{P}^{ph}$ is the minimum/maximum pumping power of the unit; $P^{pg}/P^{ph}$ is the generating/pumping power of the unit. The variation of the PSP reservoir capacity is represented by constraint (16e), where $RC$ is the storage capacity of upper reservoir; $\eta_{ph}$ and $\eta_{pg}$ are water-volume-electricity conversion coefficients during pumping and generating, respectively. Constraints (16f) enforces the upper and lower limits of the PSP reservoir capacity, where $\overline{RC}$ and $\underline{RC}$ are the upper and lower limits of the capacity of the upper reservoir. Constraint (16g) shows that at the end of the operation horizon the capacity of PSP reservoir should be equal to the capacity at the beginning. Constraints (16h–k) represent the logic relationship between the startup/shutdown indicators and the on/off state variables of the PSP units. Constraints (16l) and (16m) enforce upper limits of the upward and downward reserves of the PSP units, respectively, where $RU^{PS}$ and $RD^{PS}$ are the upward and downward reserves, respectively.

## 3.3 Modeling of power network

The DC power flow model is used to represent the power flow in transmission network (Li, 2014). The related constraints are formulated as follows.

$$P_{i,t}^{g} + P_{i,t}^{h} + \left( P_{i,t}^{pv} - \Delta P_{i,t}^{pv} \right) + \left( P_{i,t}^{wt} - \Delta P_{i,t}^{wt} \right)$$
$$+ \left( P_{i,t}^{dis} - P_{i,t}^{ch} \right) + \left( P_{i,t}^{pg} - P_{i,t}^{ph} \right) - P_{i,t}^{L} = P_{i,t} \quad \forall i \in N_d, \forall t \in T$$
$$(17a)$$

$$P_{ij,t} = \frac{\theta_{i,t} - \theta_{j,t}}{x_{ij,t}} \qquad \forall i,j \in N_d, \forall t \in T \qquad (17b)$$

$$P_{i,t} = \sum_{j \in \Phi_i} P_{ij,t} \qquad \forall i,j \in N_d, \forall t \in T \qquad (17c)$$

$$-\overline{P}_{ij} \le P_{ij,t} \le \overline{P}_{ij} \qquad \forall i,j \in N_d, \forall t \in T \qquad (17d)$$

$$\sum_{i=1}^{N_g} RU_{i,t} + \sum_{h=1}^{N_h} RU_{h,t} + \sum_{p=1}^{N_{PS}} \sum_{g=1}^{N_p^{gu}} RU_{p,g,t} \ge \Delta P_L \qquad \forall t \in T \qquad (17e)$$

$$\sum_{i=1}^{N_g} RD_{i,t} + \sum_{h=1}^{N_h} RD_{h,t} + \sum_{p=1}^{N_{PS}} \sum_{p=1}^{N_{PS}} RD_{p,g,t} \ge \Delta P_L \qquad \forall t \in T \qquad (17f)$$

Constraint (17a) describes the nodal active power balance of the network, where $P_{i,t}$ and $P_{i,t}^{L}$ are the active power injection and load of bus $i$ at time $t$, respectively. Constraints (17b) and (17c) represent the DC power flow model of the transmission network, where $x_{ij}$ is the reactance of branch between buses $i$ and $j$; $\theta_{i,t}$ is the voltage angle of bus $i$ at time $t$; $P_{ij,t}$ is active power flow on the branch between buses $i$ and $j$ at time $t$; $\Phi_i$ is the set of buses directly connected with bus $i$. Constraint (17d) imposes the power flow capacity on branches, where $\overline{P}_{ij}$ is the active power flow capacity of branch between buses $i$ and $j$. Constraints (17e) and (17f) ensure that the upward and downward reserves of power system are sufficient to handle the pre-specified power disturbance.

## 4 Multi-objective optimization-based renewable energy accommodation capacity evaluation method

Accommodating renewable energy not only needs to resolve the technical issues as previously illustrated but also needs to tackle the economic issues since it does not necessary mean the higher penetration of the renewable brings about the lower overall operational cost of the entire power system. The relationship between overall operational cost and the penetration



FIGURE 4
The relationship between the overall cost and penetration of renewable energy.
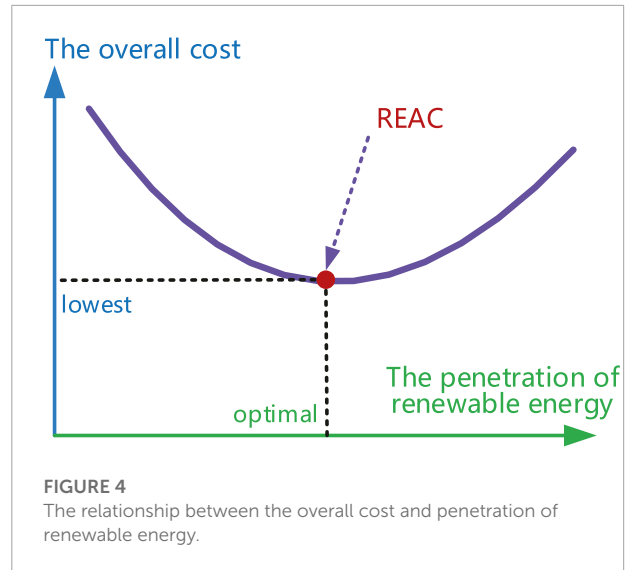
of renewable energy is illustrated in Figure 4. Intuitively, when the penetration of renewable energy is relatively low, increasing renewable energy installation will contribute to the reduction of overall operational cost as the costly thermal power is replaced by the free renewable energy generation. However, there exists a turning point where further improving renewable energy penetration no longer leads to the decline of the overall operational cost when the increment accommodation cost surpasses the extra energy cost saving. Thus, at this turning point the overall operational cost is lowest and mathematically it can be interpreted as the renewable energy accommodation capacity of the power system. To find the REAC accurately, it is necessary to establish a multi-objective optimization model considering both economic and technical issues.

### 4.1 Multi-objective optimization model

Multiple objectives need to be considered when optimizing the power system operation, including renewable energy curtailment penalty $f_1$, renewable energy units daily maintenance cost $f_2$, thermal power unit operation cost $f_3$, battery energy system degradation cost $f_4$, hydro-power plant startup/shutdown cost $f_5$, pumped storage power station startup/shutdown cost $f_6$, and the upward and downward reserve acquirement cost $f_7$, which are formulated as follows.

$$min \quad f = f_1 + f_2 + f_3 + f_4 + f_5 + f_6 + f_7 \qquad (18a)$$

$$f_1 = \sum_{t=1}^{T} \sum_{m=1}^{N_{wt}} K_{wt}^{ctl} \Delta P_{m,t}^{wt} + \sum_{t=1}^{T} \sum_{m=1}^{N_{pv}} K_{pv}^{ctl} \Delta P_{n,t}^{pv} \qquad (18b)$$

$$f_2 = \sum_{t=1}^{T} \sum_{m=1}^{N_{wt}} K_{wt} P_{m,t}^{wt} + \sum_{t=1}^{T} \sum_{m=1}^{N_{pv}} K_{pv} P_{m,t}^{pv} \qquad (18c)$$

**FIGURE 5**
Flowchart of the proposed REAC evaluation method.
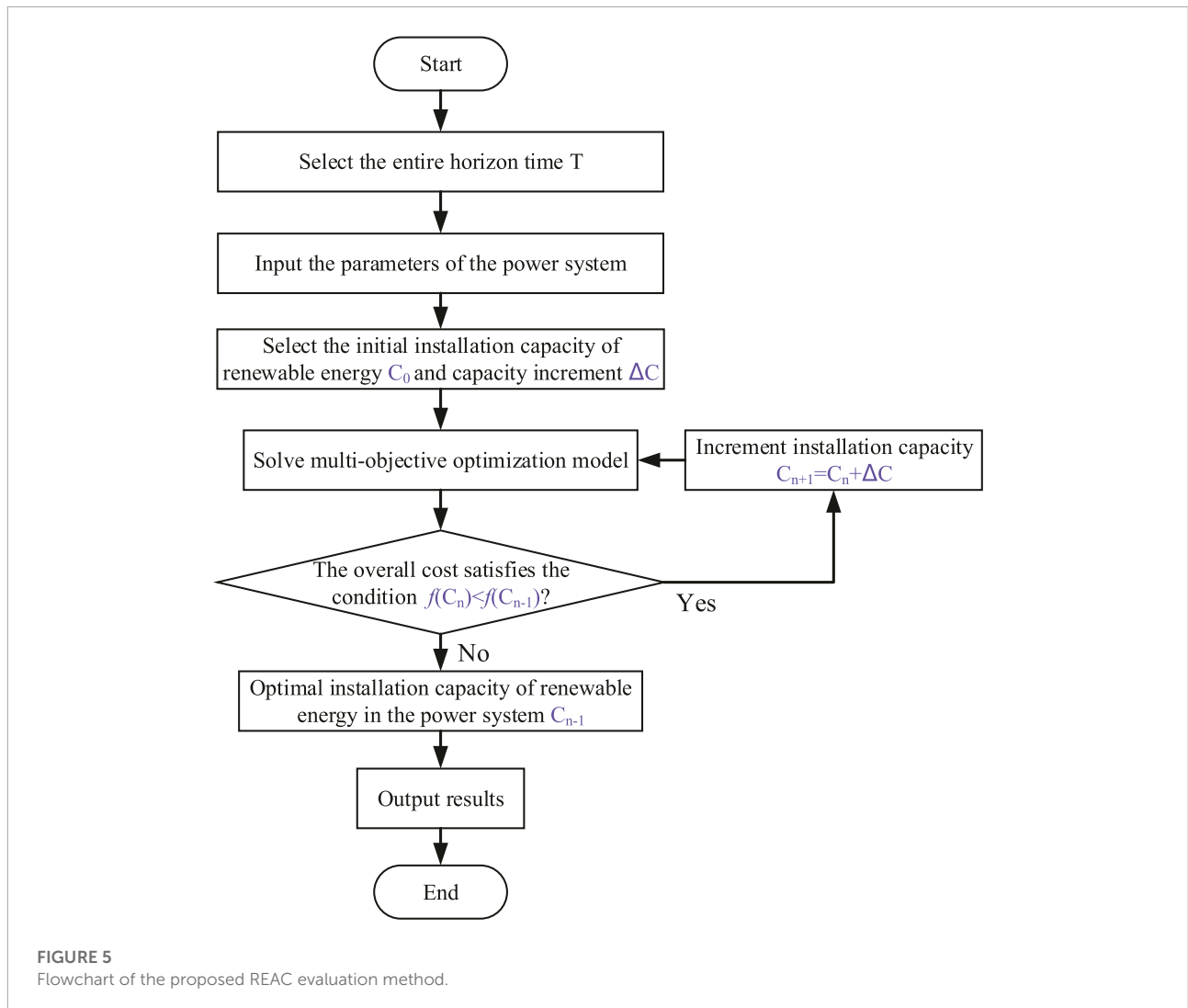
$$f_3 = \sum_{t=1}^{T}\sum_{i=1}^{N_g} F_{i,t}^g + \sum_{t=1}^{T}\sum_{m=1}^{N_g}\left(Y_{i,t}^g C_i^{SU} + Z_{i,t}^g C_i^{SD}\right) \tag{18d}$$

$$f_4 = \sum_{s=1}^{N_{BES}}\sum_{t=1}^{T} K_{s,t}^{BES}\left(P_{s,t}^{ch} + P_{s,t}^{dis}\right) \tag{18e}$$

$$f_5 = \sum_{t=1}^{T}\sum_{h=1}^{N_h}\left(Y_{h,t}^{hy} C_h^{UH} + Z_{h,t}^{hy} C_h^{DH}\right) \tag{18f}$$

$$f_6 = \sum_{t=1}^{T}\sum_{p=1}^{N_{PS}}\sum_{p=1}^{N_p^{gu}}\left(\left(Y_{p,g,t}^{pg} + Y_{p,g,t}^{ph}\right) C_{p,g}^{on}\right.$$
$$\left. +\left(Z_{p,g,t}^{pg} + Z_{p,g,t}^{ph}\right) C_{p,g}^{off}\right) \tag{18g}$$

$$f_7 = \sum_{t=1}^{T}\left\{\sum_{i=1}^{N_g}\left(C_i^{RU} RU_{i,t}^g + C_i^{RD} RD_{i,t}^g\right)\right.$$
$$+ \sum_{h=1}^{N_h}\left(C_h^{RU} RU_{h,t}^{hy} + C_h^{RD} RD_{h,t}^{hy}\right)$$
$$\left. + \sum_{p=1}^{N_{PS}}\sum_{g=1}^{N_p^{gu}}\left(C_p^{RU} RU_{p,g,t}^{PS} + C_p^{RD} RD_{p,g,t}^{PS}\right)\right\} \tag{18h}$$

where $K_{wt}^{ctl}$ and $K_{pv}^{ctl}$ are the unit penalty costs for the curtailment of WT and PV power, respectively; $K_{wt}$ and $K_{pv}$ are the maintenance cost coefficients of WT and PV, respectively; $f_3$ includes the operating cost and startup/shutdown cost considering deep peak regulation, where $C_i^{SU}$ and $C_i^{SD}$ are the unit startup and shutdown costs of TPU $i$, respectively; $K_{s,t}^{BES}$ is the unit degradation cost of BES; $C_h^{UH}$ and $C_h^{DH}$ are the unit startup and shutdown costs, respectively; $C_{p,g}^{on}$ and $C_{p,g}^{off}$ are the unit startup and shutdown costs of the unit $g$ in PSP $p$, respectively; $C^{RU}$ and $C^{RD}$ are the unit upward and downward reserves acquirement

**FIGURE 6**
The network topology of the modified IEEE 39-bus transmission system.
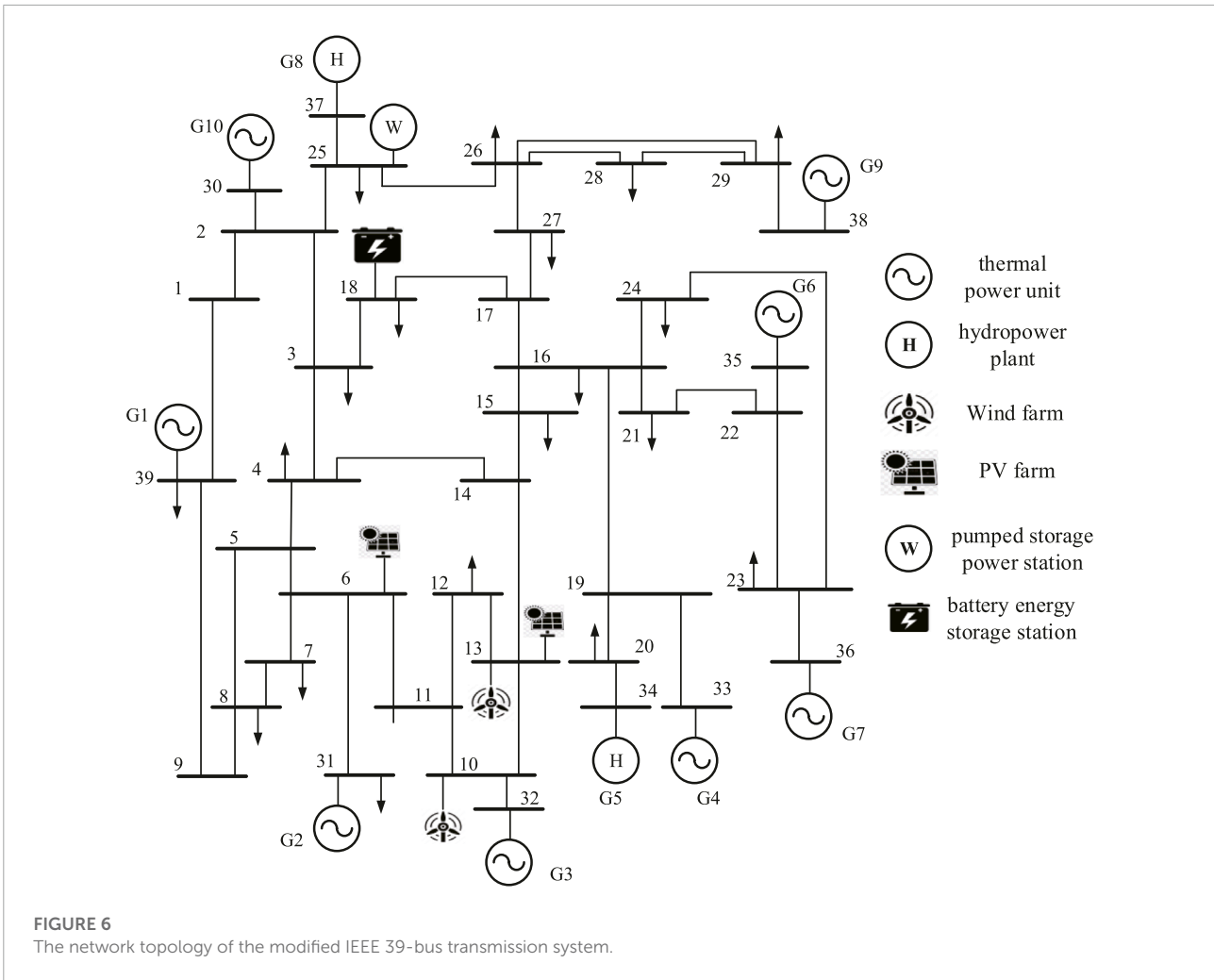
cost, respectively; $N_{wp}$, $N_{pv}$, $N_g$, $N_h$, $N_{BES}$, $N_{PS}$ are the set of wind farm, PV farm, TPU, HPP, BES and PSP, respectively; $N_p^{gu}$ is the set of the pumped generator units in PSP $p$.

Three categories of system security and operation constraints are considered as follows,

1) Constraints derived from the deep peak regulation requirement (4b), (5).
2) Constraints derive from the primary frequency response requirement (8), (9), (10).
3) Interaction model of "source-network-storage", including constraints (11), (12), (14), (15), (16), (17).

## 4.2 Incremental capacity augmentation-based renewable energy accommodation capacity evaluation

Based on the established multi-objective optimization model, we develop an novel evaluation method of REAC in

power system based on an incremental capacity augmentation approach. The flowchart of the proposed REAC method is demonstrated in **Figure 5**.

The proposed evaluation method of the REAC in power system consists of seven steps illustrated as follows,

***Step*** (***B1***) Select the entire horizon time $T$;

***Step*** (***B2***) Input the relevant parameters of the power system;

***Step*** (***B3***) Select the initial installation capacity of renewable energy $C_0$ and installation capacity increment $\Delta C$;

***Step*** (***B4***) Solve the established multi-objective optimization model by integrating the interaction of "source-network-storage" and the requirements of peak and frequency regulation.

***Step*** (***B5***) Compare the solved optimal operational cost $f(C_n)$ of this iteration with that $f(C_{n-1})$ of the last iteration. If the operation cost still declines, i.e., $f(C_n) < f(C_{n-1})$, increment the installation capacity of renewable energy by $\Delta C$ and return to ***Step*** (***B4***); otherwise, the installation capacity of renewable energy $C_{n-1}$ is recognized as the REAC of the power system.

***Step*** (***B6***) Output the REAC result.

TABLE 1  The parameters of thermal power units.

| unit | $P_i^{gN}$(MW) | $H_i^{gen}$(s) | $a_i$(\$/(MW)$^2$) | $b_i$(\$/MW) | $c_i$(\$) | $S_i^g$(\$) | $R_i^{Up}/R_i^{Dw}$(MW/h) |
|---|---|---|---|---|---|---|---|
| 1 | 1,050 | 5.0 | 0.000158*900 | 0.18*900 | 4.0*900 | 3633000 | 400 |
| 2 | 650 | 4.3 | 0.000182*900 | 0.25*900 | 5.0*900 | 2249000 | 300 |
| 3 | 750 | 4.5 | 0.000183*900 | 0.26*900 | 4.5*900 | 2595000 | 250 |
| 4 | 650 | 4.3 | 0.000178*900 | 0.25*900 | 5.0*900 | 2249000 | 200 |
| 5 | 700 | 4.5 | 0.000178*900 | 0.26*900 | 5.0*900 | 2422000 | 250 |
| 6 | 600 | 4.2 | 0.000185*900 | 0.30*900 | 4.5*900 | 2076000 | 200 |
| 7 | 850 | 4.8 | 0.000175*900 | 0.26*900 | 5.0*900 | 2941000 | 350 |
| 8 | 1,000 | 5.0 | 0.000180*900 | 0.27*900 | 6.0*900 | 3460000 | 400 |

TABLE 2  Parameters of hydropower plants, battery energy storage station and pumped storage power station.

| Battery storage power station | | Pumped storage power station | | Hydropower plant | | | |
|---|---|---|---|---|---|---|---|
| para | value | para | value | para | value | para | value |
| $\overline{SOC}_s$ | 0.9 | $\overline{RC}_p$(m$^3$) | 1332740 | $\overline{V}_h$(Hm$^3$) | 500 | $\eta_h$ | 6.465 |
| $\underline{SOC}_s$ | 0.1 | $\underline{RC}_p$(m$^3$) | 75640 | $\underline{V}_h$(Hm$^3$) | 100 | $Hd_{h,0}$ | 0.58434 |
| $C_s^{BES}$(MVA) | 600 | $\overline{P}_s^{pg}$(MW) | 4 × 200 | $\overline{Qb}_h$(Hm$^3$/h) | 40 | $\alpha_h$ | 0.00115 |
| $\overline{P}_s^{ch}$(MW) | 10 | $\overline{P}_s^{pw}$(MW) | 4 × 200 | $\underline{Qb}_h$(Hm$^3$/h) | 0 | $H_i^{gen}$(s) | 8.0 |
| $\overline{P}_s^{dis}$(MW) | 10 | $H_i^{gen}$(s) | 3.2 | $\overline{P}_h$(MW) | 500 | $K_{G,i}^{\star}$ | 40 |
| $\eta^{ch}/\eta^{dis}$ | 0.9 | $K_{G,i}$ | 28.57 | $\underline{P}_h$(MW) | 7 | $v_{h,0}$(Hm$^3$) | 300 |
| $K_s^{BES}$(\$/MW·h) | 10 | $\eta^{pw}/\eta^{pg}$ | 74.9/99.8 | $Qn_{h,t}$(Hm$^3$/h) | 5.0 | $v_{h,T}$(Hm$^3$) | 300 |
| — | — | $C_{p,g}^{on}/C_{p,g}^{off}$(\$) | 20 | $C_h^{Uh}/C_h^{Dh}$(\$) | 20 | — | — |

# 5 Numerical results

The proposed REAC evaluation method is tested on the modified IEEE 39-bus system to verify its effectiveness. All case studies are carried out on MATLAB platform using CPLEX as the MILP solver. The modified IEEE 39-bus system includes 8 TPUs, 2 HPPs, 2 wind farms, 2 PV farms, a BES and a PSP, as shown in **Figure 6**. The installation capacity of WT is set equal with that of PV, and the parameters of 2 HPPs are identical.

In the test cases, all TPUs, HPPs and PSP are enabled to provide primary frequency regulation, and all TPUs are able to provide deep peak regulation. The maximum power outputs of TPUs are their rated capacities $P_i^{gN}$. Without loss of generality, the normal minimum power output without deep peak regulation is assumed to be 0.5 times of the rated capacity, i.e., $0.5P_i^{gN}$; The minimum technical power outputs in DPR and DPRO states are assumed to be 0.4 and 0.3 times of the rated capacity, i.e., $0.4P_i^{gN}$, $0.3P_i^{gN}$, respectively. The minimum on and off times of TPUs are assumed $2h$. The per-unit values of the droop coefficients are randomly generated from 20∼ 25 with respect to the rated capacities of the TPUs. The unit penalty cost for wind power and PV power curtailment is set as 20 \$/(MW·h).

The rated frequency of the test system is 50 Hz, and the upper limit of RoCoF is chosen as 1 Hz/s. The maximum allowable frequency deviation of UFLS relay is set as ± 0.8 Hz. The quasi-steady frequency deviation limit is set as ± 0.2 Hz. Other parameters of TPUs are listed in **Table 1**, and the parameters of
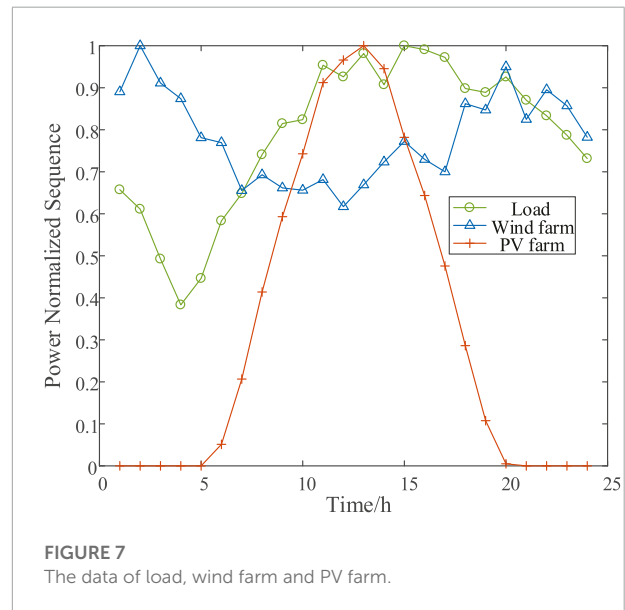


FIGURE 7
The data of load, wind farm and PV farm.

HPPs, battery energy storage power station and PSP are listed in **Table 2**. The typical daily load profile, wind and PV power output profiles are depicted in **Figure 7**.

It is known that both the tripping of the conventional generator and the realization of the forecast error of renewable energy can lead to the great power disturbance. Hence, in this paper we chose the disturbance as the larger one between the loss

**FIGURE 8**
The overall operational cost and renewable energy consumption rate with different total renewable energy installation capacities.
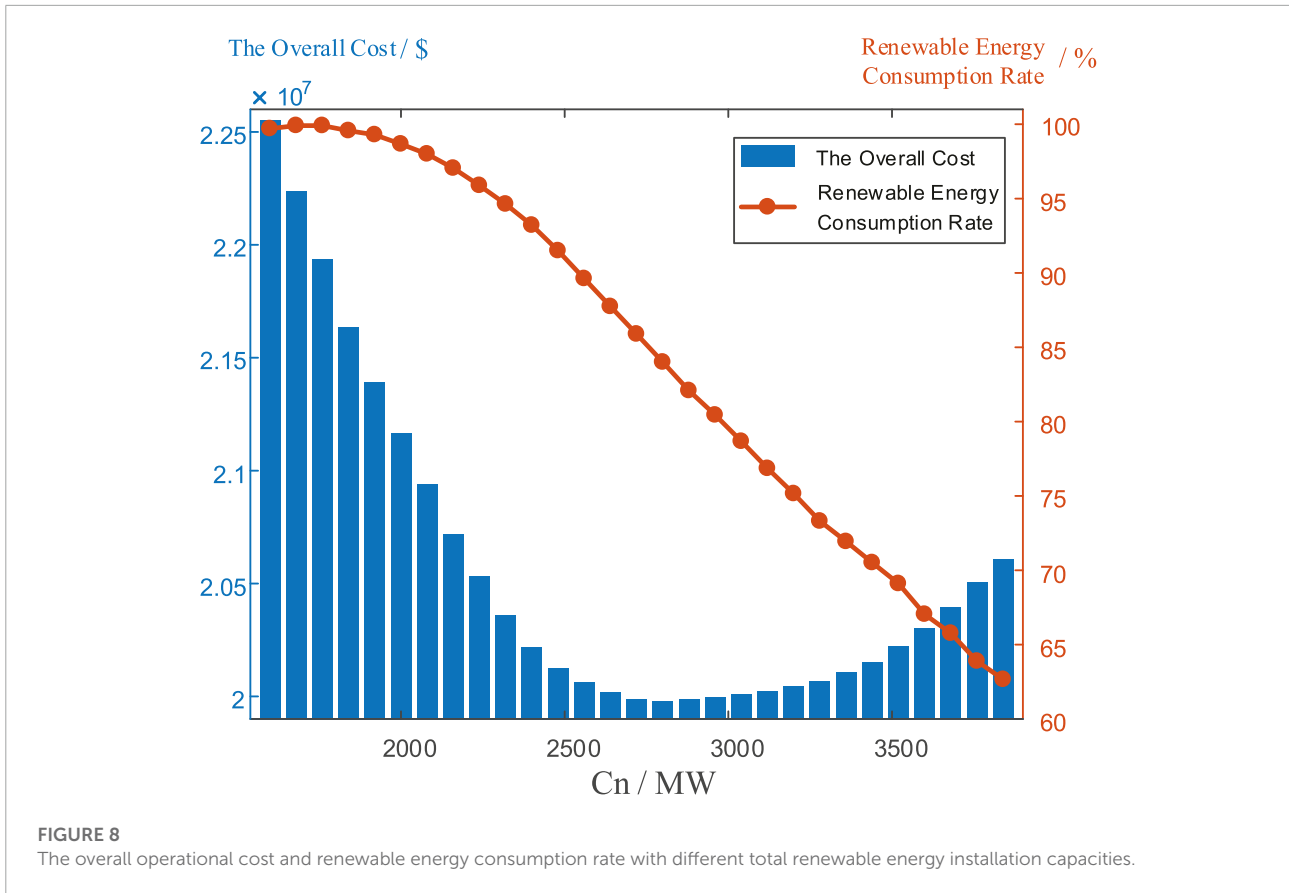
of the largest generation unit and the conservative estimation of the total renewable energy forecast error which is set as ± 30% of the total predicated renewable energy output.

## 5.1 Effectiveness of the proposed evaluation method

In this subsection, the effectiveness of the proposed REAC evaluation method is verified on the modified IEEE 39-bus test system. Here, the initial installation capacity of renewable energy $C_0$ is equal to $1600\ MW$ and installation capacity increment $\Delta C$ is equal to $80\ MW$. **Figure 8** depicts the relationship between the overall operational cost of the system and the total renewable energy installation capacity as well as the relationship between the renewable energy accommodation rates of the system and the total renewable energy installation capacity. **Figure 9** demonstrates the accommodated wind/PV energy and generated energy of TPUs under different total renewable energy installation capacities.

It can be observed from **Figure 8**, with the growth of total renewable energy installation capacity, the overall operational cost declines first as a portion of TPU power output is replaced by the renewable energy output as demonstrated

in **Figure 9**. The overall operational cost reaches the lowest value given $Cn = 2800\ MW$ and then starts to augment with further growth of the total renewable energy installation capacity as the REAC become saturated. The reason is that the system requires sufficient conventional generators to provide frequency response regulation support and thus the further expanding the total renewable energy capacity only results in the increased curtailment rather than the replacement of TPU as show in **Figures 8**, **9**. Therefore, $Cn = 2800\ MW$ is considered as the renewable energy accommodation capacity of the test system since at this point the overall operational cost is lowest, which verifies the effectiveness of the proposed method.

## 5.2 Performance comparison

In this subsection, the superiority of the proposed REAC evaluation method considering both peak and frequency regulation, is validated through the comparison with three benchmark schemes. The first benchmark scheme considers neither peak regulation nor frequency regulation, denoted as S1. The second benchmark scheme only considers peak regulation, denoted as S2, and the last benchmark scheme only considers
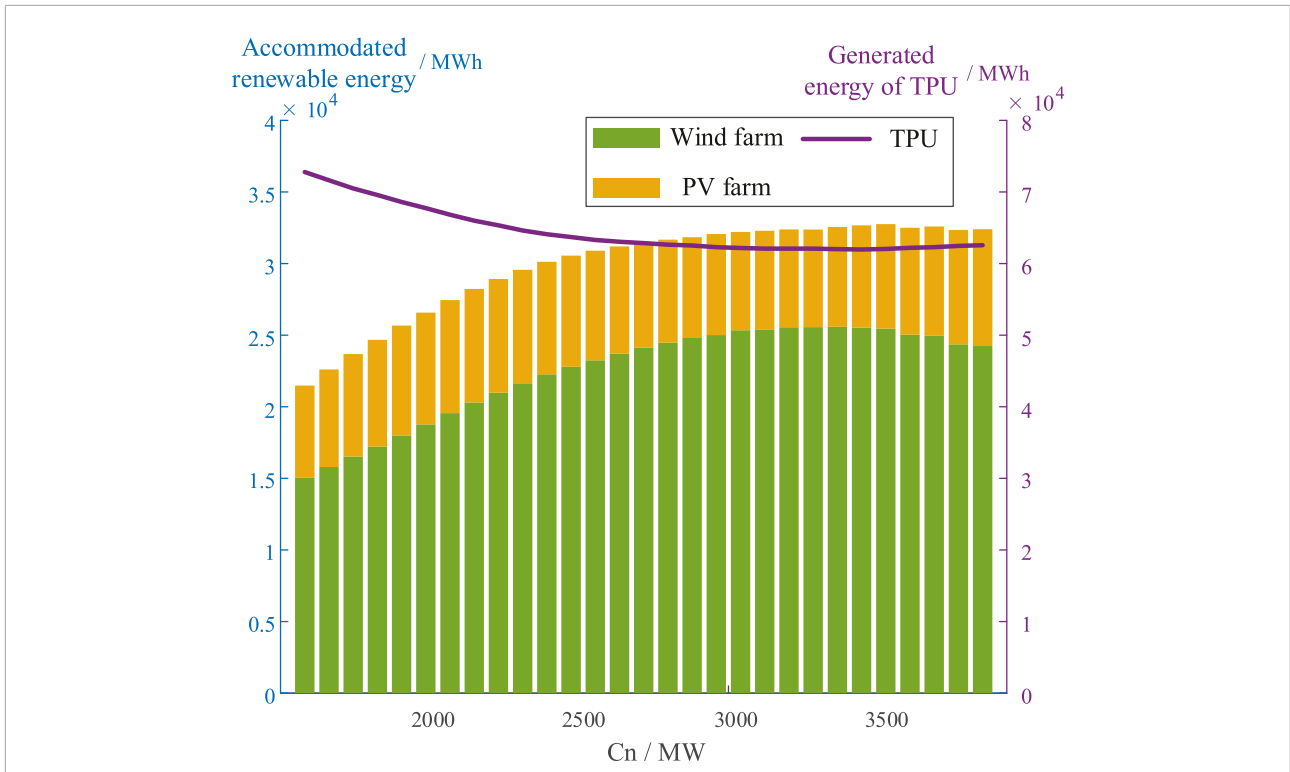
**FIGURE 9**
The accommodated PV/Wind energy and generated energy of TPU with different total renewable energy installation capacities.
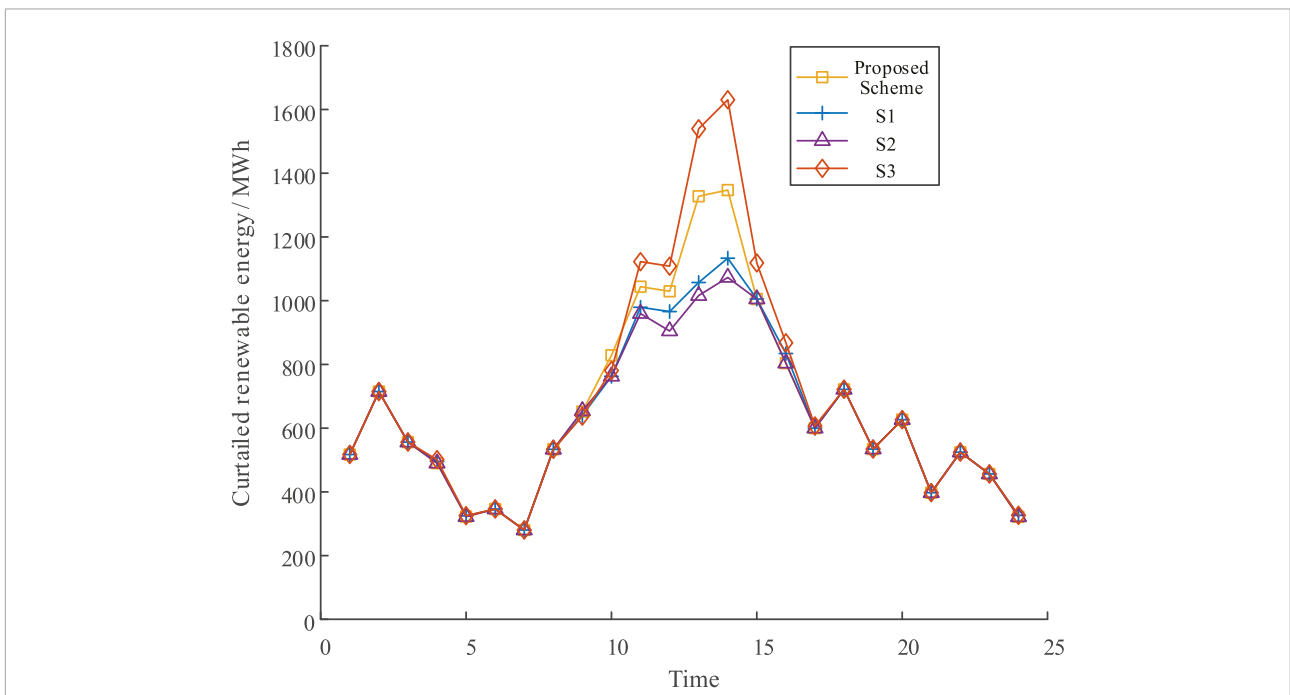


**FIGURE 10**
The curtailment of renewable energy with different schemes.

TABLE 3 The operation cost and renewable energy accommodation rate using different schemes.

| Scheme | Overall operational cost $f$($) | Curtailment cost $f_1$($) | Other costs $\sum_{i=2}^{7} f_i$($) | Renewable energy accommodation rate |
|---|---|---|---|---|
| Proposed | $2.0302 \times 10^7$ | 319610.3693 | $1.9982 \times 10^7$ | 67.0397% |
| S1 | $2.0105 \times 10^7$ | 306652.7749 | $1.9798 \times 10^7$ | 68.3760% |
| S2 | $1.9866 \times 10^7$ | 302428.6012 | $1.9564 \times 10^7$ | 68.8116% |
| S3 | $2.0902 \times 10^7$ | 335478.5843 | $2.0566 \times 10^7$ | 65.4033% |

frequency regulation, denoted as S3. The installation capacity of each wind farm and PV farm is set as 900 MW in all schemes.

Table 3 summarizes the comparison of the operation cost and renewable energy accommodation rate of different schemes. As shown in the table, the overall cost of scheme S3 is largest, which is followed by the proposed scheme and S1, and S2 yields the lowest overall cost. The ranking order of the renewable energy accommodation rate of the four schemes is exactly reversed, which means the higher accommodation rate gives rise to the lower overall cost. Figure 10 shows the renewable energy curtailment profiles using different schemes. It is shown that the curtailment is highest during the period of the renewable energy peak generation. Moreover, S3 has the highest curtailment and S2 yields the lowest curtailment, which is consistent with the results in Table 3. Hence, we can conclude from the above results the considering deep peak regulation is beneficial for the renewable energy accommodation and incorporating the frequency regulation inhibits the renewable energy accommodation. The reason is that when deep peak regulation is considered, the minimum power output of TPUs can be further lowered leading the improvement of the power system flexibility and hence promoting the renewable energy accommodation. When the frequency response requirement is taken into account, the system requires sufficient generators online to maintain the required inertia level and to provide sufficient reserve to handle power disturbance, which squeezes the renewable energy hosting capacity of the power system and thus causing higher wind and PV power curtailment. Therefore, it is necessary to consider both the peak regulation and frequency regulation in order to obtain the accurate outcome of the REAC evaluation since both regulations are the fundamental part of the power system operation and have considerable impact on the renewable energy accommodation.

## 6 Conclusion

In this paper, a novel REAC evaluation method is developed for power systems considering peak and frequency regulation as well as the "source-network-storage" interaction. First, the peak and frequency regulation response model is established and simplified to reduce the computational complexity. Then, according to the interaction of "source-network-storage", a daily

power system operational model is constructed. Furthermore, a multi-objective optimization model is proposed considering both economic and technical issues, and an novel evaluation REAC method is developed based on the incremental capacity augmentation technique. Finally, the numerical tests on the modified IEEE 39-bus system verify the effectiveness of the proposed method.

## Data availability statement

The data analyzed in this study is subject to the following licenses/restrictions: The dataset involve commercial privacy. Requests to access these datasets should be directed to zycy@hnu.edu.cn.

## Author contributions

YY conceptualized the study, contributed to the study methodology, and wrote the original draft. HZ contributed to the writing-review and editing, data curation and investigation. YZ contributed to study methodology, data analysis, wrote the original draft and writing-review. DY contributed to software and data analysis. BW contributed to investigation and writing-original draft. QX contributed to supervision and writing-review and editing. BL contributed to software and paper revision. All authors have read and agreed to the published version of the manuscript.

## Conflict of interest

Authors YY, HZ, FC, DY, BW, and QX were employed by State Grid Hubei Electric Power Co., Ltd.

The authors declare that this study received funding from science and technology project of State Grid

Hubei Electric Power Company Limited. The funder had the following involvement in the study: data curation, investigation, the study methodology, software and data analysis, writing the original draft and the writing-review & editing.

The remaining authors declare that the research was conducted in the absence of any commercial or financial relationships that could be construed as a potential conflict of interest.

## Publisher's note

## References

Alves, E. F., Mota, D. d. S., and Tedeschi, E. (2021). Sizing of hybrid energy storage systems for inertial and primary frequency control. *Front. Energy Res.* 206, 649200. doi:10.3389/fenrg.2021.649200

Babayev, D. A. (1997). Piece-wise linear approximation of functions of two variables. *J. Heuristics* 2, 313–320. doi:10.1007/bf00132502

Carrión, M., and Arroyo, J. M. (2006). A computationally efficient mixed-integer linear formulation for the thermal unit commitment problem. *IEEE Trans. Power Syst.* 21, 1371–1378. doi:10.1109/tpwrs.2006.876672

Carrión, M., Dvorkin, Y., and Pandžić, H. (2018). Primary frequency response in capacity expansion with energy storage. *IEEE Trans. Power Syst.* 33, 1824–1835. doi:10.1109/TPWRS.2017.2735807

Chávez, H., Baldick, R., and Sharma, S. (2014). Governor rate-constrained opf for primary frequency control adequacy. *IEEE Trans. Power Syst.* 29, 1473–1480. doi:10.1109/tpwrs.2014.2298838

Chen, Z., Wu, L., and Shahidehpour, M. (2014). Effective load carrying capability evaluation of renewable energy via stochastic long-term hourly based scuc. *IEEE Trans. Sustain. Energy* 6, 188–197. doi:10.1109/tste.2014.2362291

Gao, Y., Zeng, D., Zhang, L., Hu, Y., and Xie, Z. (2020). Research on modeling and deep peak regulation control of a combined heat and power unit. *IEEE Access* 8, 91546–91557. doi:10.1109/ACCESS.2020.2993279

Guan, H., Feng, Y., Yang, X., Du, Y., Feng, D., and Zhou, Y. (2022). Optimization strategy of combined thermal-storage-photovoltaic economic operation considering deep peak load regulation demand. *Energy Rep.* 8, 112–120. doi:10.1016/j.egyr.2022.03.050

Guo, Z., Zhang, X., Feng, S., and Zhang, H. (2020). The impacts of reducing renewable energy subsidies on China's energy transition by using a hybrid dynamic computable general equilibrium model. *Front. Energy Res.* 8, 25. doi:10.3389/fenrg.2020.00025

He, W., Gao, Q., and Chen, Y. (2018). "Evaluation on renewable energy accommodation ability based on peak load regulation and capacity constraint," in 2018 International Conference on Power System Technology (POWERCON), Guangzhou, China, November 6–8, 2018, (IEEE), 905–910.

Khalkho, A. M., Rapada, B., Majumder, G., Cherukuri, M., and Mohanta, D. K. (2022). Impact assessment of solar power generation uncertainty on smart grid reliability and carbon neutrality. *Front. Energy Res.* 10, 220. doi:10.3389/fenrg.2022.851449

Kushwaha, P., Prakash, V., Bhakar, R., Yaragatti, U. R., Jain, A., and Sumanth, Y. (2018). Assessment of energy storage potential for primary frequency response adequacy in future grids," in 2018 8th IEEE India International Conference on Power Electronics (IICPE), Jaipur, India, December 13–15, 2018, (IEEE), 1–6.

Li, H., Wang, Y., Zhang, X., and Fu, G. (2021). Evaluation method of wind power consumption capacity based on multi-fractal theory. *Front. Energy Res.* 9, 634551. doi:10.3389/fenrg.2021.634551

Li, W. (2014). *Risk assessment of power systems: Models, methods, and applications*. Vancouver, Canada: John Wiley & Sons.

Lin, K., Lu, X., Wu, F., and Shi, L. (2020). "Evaluation of the renewable energy accommodation capacity in the regional power grid," in 2020 12th IEEE PES Asia-Pacific Power and Energy Engineering

Conference (APPEEC), Nanjing, China, September 20–23, 2020 (IEEE), 1–4.

Liu, Y., Wu, L., Yang, Y., Chen, Y., Baldick, R., and Bo, R. (2021). Secured reserve scheduling of pumped-storage hydropower plants in iso day-ahead market. *IEEE Trans. Power Syst.* 36, 5722–5733. doi:10.1109/tpwrs.2021.3077588

Majeed, A., Ahmad, M., Rasheed, M. F., Khan, M. K., Popp, J., and Oláh, J. (2022). The dynamic impact of financial globalization, environmental innovations and energy productivity on renewable energy consumption: Evidence from advanced panel techniques. *Front. Environ. Sci.* 447, 894857. doi:10.3389/fenvs.2022.894857

Tan, J., and Zhang, Y. (2017). Coordinated control strategy of a battery energy storage system to support a wind power plant providing multi-timescale frequency ancillary services. *IEEE Trans. Sustain. Energy* 8, 1140–1153. doi:10.1109/tste.2017.2663334

Teng, F., and Strbac, G. (2016). Assessment of the role and value of frequency response support from wind plants. *IEEE Trans. Sustain. Energy* 7, 586–595. doi:10.1109/tste.2015.2505085

Wang, C., Bie, Z., Yan, C., Li, Z., Liu, F., Ding, K., et al. (2016). Evaluation of power grids' renewable energy accommodation capacity considering wind power and photovoltaic power. *IEEE PES Asia-Pacific Power Energy Eng. Conf.*, 1518–1522. doi:10.1109/APPEEC.2016.7779744

Wang, C., Liu, S., Bie, Z., and Wang, J. (2018). Renewable energy accommodation capability evaluation of power system with wind power and photovoltaic integration. *IFAC-PapersOnLine* 51, 55–60. doi:10.1016/j.ifacol.2018.11.677

Wen, Y., Li, W., Huang, G., and Liu, X. (2016). Frequency dynamics constrained unit commitment with battery energy storage. *IEEE Trans. Power Syst.* 31, 5115–5125. doi:10.1109/tpwrs.2016.2521882

Wu, L., Shahidehpour, M., and Li, Z. (2008). Genco's risk-constrained hydrothermal scheduling. *IEEE Trans. Power Syst.* 23, 1847–1858. doi:10.1109/tpwrs.2008.2004748

Xia, P., Deng, C., Chen, Y., and Yao, W. (2019). Milp based robust short-term scheduling for wind–thermal–hydro power system with pumped hydro energy storage. *IEEE Access* 7, 30261–30275. doi:10.1109/access.2019.2895090

Xie, J., Wang, K., Feng, D., Zeng, D., Li, Y., and Yue, D. (2016). A security-constrained flexible demand scheduling strategy for wind power accommodation. *Int. Trans. Electr. Energy Syst.* 26, 1171–1183. doi:10.1002/etep.2123

Xu, Q., Kang, C., Zhang, N., Ding, Y., Xia, Q., Sun, R., et al. (2014). A probabilistic method for determining grid-accommodable wind power capacity based on multiscenario system operation simulation. *IEEE Trans. Smart Grid* 7, 400–409. doi:10.1109/tsg.2014.2381271

You, F., Si, X., Dong, R., Lin, D., Xu, Y., and Xu, Y. (2022). A state-of-charge-based flexible synthetic inertial control strategy of battery energy storage systems. *Front. Energy Res.* 603, 908361. doi:10.3389/fenrg.2022.908361

Zhang, G., Ela, E., and Wang, Q. (2018). Market scheduling and pricing for primary and secondary frequency reserve. *IEEE Trans. Power Syst.* 34, 2914–2924. doi:10.1109/tpwrs.2018.2889067

Zhang, X., Wang, J., Wang, Y., Zou, M., and Ning, Y. (2019). "Consumption capability of renewable energy based on network maximum flow model," in Proceedings of the 2nd International Conference on Information Technologies and Electrical Engineering, Zhuzhou, China, December 6–7, 2019, 1–6.